ISSN 1330-3651 (Print), ISSN 1848-6339 (Online)
https://doi.org/10.17559/TV-20230704000784
Original scientific paper

Parameter Optimization and Test of High-Speed Plough Based on Coupling EDEM and Recurdyn

Xin ZHENG*, Wenbao XU, Hengyan XIE

Abstract: Depress moldboard plow soil adhesion is gaining relevance in agricultural production due to its rising profitability for producers and its contribution to reducing environmental impacts. This study aimed at the effects of the different structural forms with moldboard plow soil adhesion on adhesion under the joint simulation system. The experiment was conducted at Qianjin in the village of Qianjin, municipality of Daqing, Heilongjiang, China. Using EDEM and Recurdyn to simulate the selected parameters and operating conditions, determine the optimal combination, the field test and simulation comparison verification, the association between. The optimized plough body structure resulted in a 10.86% decrease in the soil adhesion compared to the control, providing a viable alternative for moldboard plow soil adhesion.

Keywords: coefficient of variation; moldboard plow; recurdyn

1 INTRODUCTION

The main working part of the plough is the ploughshare [1]. During ploughing, the ploughshare invades the soil under the combined action of self - weight and hydraulic pressure, and traction force act to squeeze and push the ploughshare edge to loosen the soil and thus achieve the purpose of soil breaking. The forces on the ploughshare in the soil were very complex [2-4] and were influenced by quite a few factors, including the curved shape of the ploughshare (which mainly affects the distribution of earth pressure), the adhesion, density and particle size of the soil [5-7]. Many domestic and foreign research scholars have analyzed the forces on ploughshares in soil and have obtained some important conclusions. Used theoretical mechanics to analyze the force on the ploughshare edge before and after wear by constructing a spatial force system and explored the relationship between the total ploughshare edge resistance and coefficients such as soil specific resistance, soil-metal friction coefficient, share surface angle, and pushing angle during tillage [8]. Xu Feng [9] reviewed three representations of force analysis of the plowshare: the sextant force method, the three-plane method and the force spiral method, and used the sextant force method to conduct the strength analysis of the plough frame of the plough. Lixin Zhai [1] constructed two-sided wedge and three-sided wedge models respectively in order to analyze the pressure distribution of the spar blade in the soil, and obtained the frontal resistance on the spar blade using the analytical method, but the influence of soil friction was not considered in the model, which led to a large difference among the results and the actual, and only qualitatively analyzed the influence of the angle of the plowshare into the soil on the pressure distribution on the surface of the spar blade. Liao Li et al [10] obtained the pressure distribution during plowing of the plowshare by using s-Dyna to simulate the dynamics of the plow body surface in the plowing phase of the field work process. The working surface of the plow body is a complex geometric surface, and the soil itself is not a continuously and uniformly changing medium; the motion trajectory of the tilled soil mat along the plow body surface is spatially curved. Thus, the forces on the plough body in the working state are complex [11].

2 FORCE ANALYSIS OF THE SPAR PLOUGH

2.1 Force Analysis of Plough Body

In general, the force on a plow surface is a spatially non-confluent arbitrary force system with six degrees of freedom, which cannot simply be synthesized into a single resultant force. From theoretical mechanics, it is known that any spatial force system can always be reduced to a combined force section and a combined force distance benefit, and decomposing R and M along the right-angle coordinate system X, Y, and Z axes, we can get six partial forces R_x, R_y, R_z, M_x, M_y, and M_z [8, 12-16] is shown in Fig. 1. According to the force translation theorem, the three forces can be translated so that they converge at a point, and a total resultant force can be synthesized.

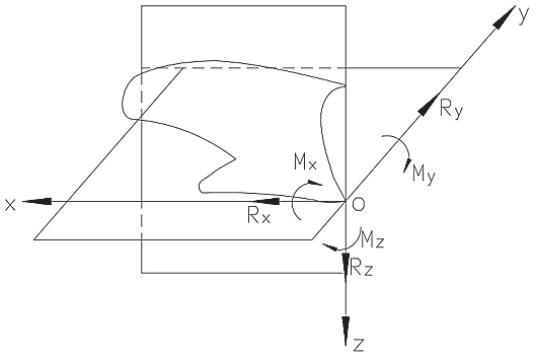

Figure 1 The plow body was tried

Since the surfaces of the plowshare are exceptionally complex and diverse, this paper directly cites the relevant assumptions and the derivation process in study of [17] to simplify the simplified model of plow-soil interaction mechanics into a two-dimensional model, and the plow-soil mechanics model is shown in Fig. 2 [18].

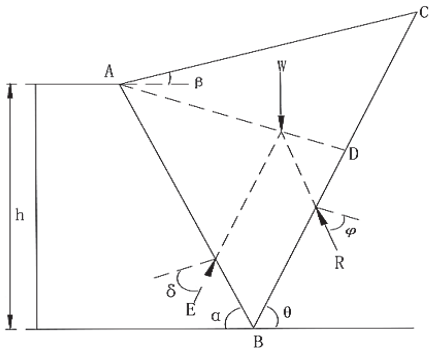

Figure 2 Plough-Soil Modes

Here the plow is simplified as a wedge, the height is h, the angle of entry is *a*, the soil is non-cohesive soil ($c = 0$), the surface of the soil body and the horizontal angle is β, the friction angle between the plowshare edge and the soil body is δ, at the uniform speed plowing process of the plowshare plow, the soil body under the action of the shear force of the plowshare edge will be displaced (translation or rotation) in the direction away from the main body, and finally the soil body is in ultimate equilibrium, the soil body will be cut in the form of a sliding soil wedge, its slip crack surface is plane *BC*, the angle between the slip crack surface and the horizontal surface into θ angle.

Before the force analysis, the following basic assumptions are made in this paper:

1) The soil is an ideal bulk particle (no cohesion).

2) The soil body sliding away is in the form of a wedge, and the sliding surface is in the same plane with the plow blade.

3) The sliding wedge (soil body) is a rigid body; do not consider the internal stress and deformation of the sliding wedge body set the forward direction of the plowshare as the *x*-axis, take the sliding soil wedge *ABC* for the isolated body, the force acting on the sliding soil wedge has the self-weight of the soil wedge body *W*, slip cracking surface *BC* on the reaction force *R* and the plow blade face of the soil wedge reaction force *E* (the soil body acting on the plow blade soil pressure and *E* equal in size and direction). Sliding earth wedge in the role of *W*, *R*, *E* divided by the state of equilibrium, so the three forces must form a closed force vector triangle, by the sine theorem can be known that the reaction force *E* of the earth wedge is:

$$E = W\frac{\sin(\theta-\varphi)}{\sin(\theta-\varphi+\psi)} \tag{1}$$

Where : $\psi = \alpha - \delta$

And the self-weight of the soil is:

$$W = \gamma S_{\Delta ABC} = \frac{1}{2}\gamma \overline{BC}\cdot\overline{AD} \tag{2}$$

Where: γ is the soil gravity density and $S_{\Delta ABC}$ is the area triangle *ABC*.

In the triangle *ABC*, using the cosine theorem, we get that:

$$\overline{BC} = \overline{AB}\cdot\frac{\sin(\alpha+\beta)}{\sin(\theta-\beta)} \tag{3}$$

Also by:

$$\overline{AB} = \cdot\frac{h}{\sin\alpha} \tag{4}$$

Therefore:

$$\overline{BC} = \frac{h\cdot\sin(\alpha+\beta)}{\sin\alpha\cdot\sin(\theta-\beta)} \tag{5}$$

In triangle *ADB*, from the sine theorem, it follows that:

$$\overline{AD} = \overline{AB}\sin(\pi-(\theta+\alpha)) = \overline{AB}\sin(\theta+\alpha) \tag{6}$$

Therefore:

$$\overline{AD} = \frac{h\sin(\theta+\alpha)}{\sin\alpha} \tag{7}$$

Thus, the self-weight of the earth wedge can be further expressed as:

$$W = \frac{1}{2}\gamma h^2\frac{\sin(\alpha+\beta)\sin(\theta+\alpha)}{\sin^2\alpha\cdot\sin(\theta-\beta)} \tag{8}$$

Substituting Eq. (8) into Eq. (1), the reaction force E of the soil wedge is obtained as:

$$W = \frac{1}{2}\gamma h^2\frac{\sin(\alpha+\beta)\sin(\theta+\alpha)\sin(\theta-\varphi)}{\sin^2\alpha\sin(\theta-\beta)\sin(\theta-\varphi+\psi)} \tag{9}$$

The most dangerous slip angle between the horizontal plane $\theta_0 = 45^\circ + \varphi/2$, the θ_0 substitution Eq. (9) is:

$$\frac{\mathrm{d}E}{\mathrm{d}\theta} = 0 \tag{10}$$

The obtained most dangerous slip crack angle and the horizontal plane angle $\theta_0 = 45^\circ + \varphi/2$, the θ_0 substituted into the Eq. (9) has:

$$E_{\max} = \frac{1}{2}\gamma h^2 K_a \tag{11}$$

where K_a is called the Coulomb active earth pressure coefficient, and its value is:

$$K_a = \frac{\sin^2(\alpha+\varphi)}{\sin^2\alpha\sin(\alpha-\delta)\left[1+\sqrt{\dfrac{\sin(\varphi+\delta)\sin(\varphi-\beta)}{\sin(\alpha-\delta)\sin(\alpha+\beta)}}\right]}.$$

Thus, the pressure and shear forces acting on the ploughshare by the soil are:

$$F_n = E_{\max}\cos\delta \tag{12}$$

$$F_\tau = E_{\max}\sin\delta \tag{13}$$

2.2 The Traction Resistance of the Plow

Goryachkin, academician of the former Soviet Academy of sciences, is the founder of agricultural mechanical mechanics, and has created a series of theories, experimental calculation methods and experimental data processing methods in agricultural machinery, and the Goryachkin model created by academician Goryachkin is widely used to solve the resistance of soil acting on the plough body during tillage. Li Xia [19] (2005) used the Goryachkin model when studying the plough frame, and attributed this resistance to the following three aspects:
(1) The cutting force required for the soil breaking and flipping is F_1.
(2) The friction between the bottom and side plates of the plough and the soil that is in contact with the soil during the tillage process is F_2.
(3) The force required to generate movement after turning the broken ridge to the sides is F_3.

For the resistance of the above three parts, the calculation formula of traction resistance given by Academician Goryachkin is:

$$F_1 = kab \tag{14}$$

$$F_2 = fG \tag{15}$$

$$F_3 = eabV^2 \tag{16}$$

This gives the total traction resistance as:

$$F = F_1 + F_2 + F_3 \tag{17}$$

Among them: k is the plough resistance ratio, a is the plough ploughing width, b is the plough ploughing depth, f is the comprehensive friction, G is the total weight of the ploughshare, ε is the dynamic resistance coefficient related to the surface shape and soil properties of the plow, v is the working speed of the ploughshare, and F is the total drag resistance. When influencing the working performance of plough surfaces based on dynamic simulation, the percentage of traction resistance obtained by field tillage experiment is shown in Tab. 1:

Table 1 Percentage of the traction resistance

Traction resistance fraction	Percentage / %
Cutting force F_1	60 ～ 70
Friction F_2	25 ～ 28
Force generated by crushed soil monopoly turn F_3	13 ～ 16

Provided that the effects produced by the second and third terms are ignored, a simple formula for calculating the traction resistance can be obtained:

$$F = kab \tag{18}$$

2.3 Determination of Structural Parameters of High-Speed Plow Body

2.3.1 The Working Principle of Three-Sided Wedge

The process of plow body operation, because itself is a complex torsional surface structure, so in the process of carrying out operations, subject to the plow in no direction, in order to better be able to study the forces on the surface of the plow body, by taking micro three-sided wedge unit body of the plow body, the motion of the plow body is simplified to the motion of the three-sided wedge, which can be formed according to the different angles between each surface and the horizontal direction of α wedge, β wedge, γ wedge composed of A group of composite motion. In the process of plow operation, the forces in the three directions are the same as their own role, the role of the longitudinal wedge is mainly to start the soil and break the soil fa, the role of the horizontal wedge is to push the soil fa to the furrow side the role of the horizontal wedge is: to turn the soil fa up and placed in a certain position, these three parts can also be seen as the completion of the plow body on the soil extrusion, cutting and turning three goals. The main purpose of the analysis of the three-sided wedge is to understand the forces corresponding to the three-sided wedge in the process of soil cutting operation. In the process of force analysis, the forces on the three-sided wedge are mainly caused by the three force directions on the soil body, as shown in Fig. 3.

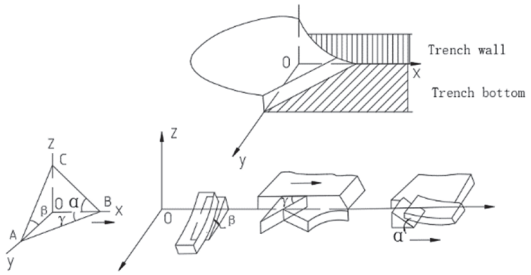

Figure 3 Force analysis of plough body operation

The three-sided wedge ABC is located in the coordinate system $Oxyz$, and the relationship between the three wedge angles can be obtained as shown below:

$$\tan\alpha = \frac{OC}{OB},\ \tan\beta = \frac{OC}{OA},\ \tan\gamma = \frac{OA}{OB} \tag{19}$$

So it can be obtained:

$$\tan\alpha = \tan\beta\ \tan\gamma \tag{20}$$

2.3.2 Force Analysis of Plow Body Model of Spar Plow

In the process of operation, the plow which is subjected to the resistance from the soil mainly consists of the following four parts: (1) the share blade is cutting the resistance of the soil body. (2) the pressure on the plowshare from the soil is being squeezed and deformed in the process of moving forward. (3) The frictional resistance of the soil in contact with the plow body as it advances.
a) The force on the cutting action of the spar blade

In the process of soil cutting, the force on the spar blade is mainly composed of two parts: one is the static force on the soil for shear damage, and the other part is the squeezing force on the plow blade after cutting the soil for the soil transport process summary.

(1) Static force on the spar blade cutting through the soil [21-25].

$$\begin{cases} N_1 = 7.2\times\dfrac{\cos^2\delta}{\sin\gamma}\int_{s1}^{\frac{\pi}{2}}\left(\sin\varepsilon + f\sin\gamma\dfrac{\cos^2\varepsilon}{\sqrt{1-\sin^2\gamma\sin^2\varepsilon}}\right)p(\varepsilon)\,\mathrm{d}\varepsilon \\ T_1 = 3.6\dfrac{\sin 2\delta}{\tan\gamma}\int_{s1}^{\frac{\pi}{2}}\dfrac{p(\varepsilon)}{\sqrt{1-\sin^2\gamma\sin^2\varepsilon}}\mathrm{d}\varepsilon \end{cases} \tag{21}$$

(2) Pressure of the soil on the spar blade [21-25].

$$\begin{cases} N_2 = 0.992\times\sin\gamma\int_{s1}^{\frac{\pi}{2}}\left(\sin\varepsilon + f\sin\gamma\dfrac{\cos^2\varepsilon}{\sqrt{1-\sin^2\gamma\sin^2\varepsilon}}\right)p(\varepsilon)\,\mathrm{d}\varepsilon \\ T_2 = 0.335\sin 2\gamma\int_{s1}^{\frac{\pi}{2}}\dfrac{\sin^2\varepsilon\, p(\varepsilon)}{\sqrt{1-\sin^2\gamma\sin^2\varepsilon}}\mathrm{d}\varepsilon \end{cases} \tag{22}$$

For the total cutting force S of the spar blade by the coordinate axis of the division of the force is equal to:

$$\begin{cases} S_x = (T_1+T_2)\cos\gamma + (N_1+N_2)\sin\gamma \\ S_y = (T_1+T_2)\sin\gamma - (N_1+N_2)\cos\gamma \\ S_z = 0 \end{cases} \tag{23}$$

b) Total soil pressure on the plowshare

The total pressure of the soil on the ploughshare [26-29] is calculated as shown below:

$$\begin{cases} P_x = \dfrac{1}{2}ks^2\sin\varepsilon\sin\gamma \\ P_y = \dfrac{1}{2}ks^2\sin\varepsilon\cos\gamma \\ P_z = \dfrac{1}{2}ks^2\cos\varepsilon \end{cases} \tag{24}$$

As can be seen from the above equation, P is related to the angles ε and γ, i.e. the force on the plow blade during travel is related to the mounting angle of the plowshare and the pushing angle.

c) Overcome the resistance caused by the friction between the soil and the ploughshare and the plough wall

The Eq. (26) to Eq. (29) for calculating the effect of the frictional resistance during the operation of the plow are shown below:

$$\begin{aligned} \mathrm{R} &= \frac{1}{\cos\beta\text{-}f\sin\beta}T_m = \\ &= \frac{1}{\cos\beta\text{-}f\sin\beta}\left[(T_0+fI)e^{f\theta} + f\left(\frac{ab\gamma}{g}v_e{}^2\sin\varepsilon\sin\gamma + \frac{1}{2}ks^2\right)\right] \end{aligned} \tag{25}$$

where f is the coefficient of friction between the soil and the plow body, I is the uniform normal load that presses the soil fa against the plow wall, v_e is the implicate motion of the soil particles and θ is the angle between the horizontal section and the forward direction, and k is the soil property.

d) The force required to make the soil move

The force [26-29] required to give the soil grain velocity is calculated:

$$\begin{cases} Q_x = \dfrac{ab\gamma}{g}v_e{}^2(1-\phi\cos\beta') \\ Q_y = -\phi\dfrac{ab\gamma}{g}v_e{}^2\sin\alpha'\sin\beta' \\ Q_z = \phi\dfrac{ab\gamma}{g}v_e{}^2\cos\alpha'\sin\beta' \end{cases} \tag{26}$$

where α is the tillage depth, β is the tillage width, and φ is the compression coefficient.

It can be concluded that the total resistance in the horizontal direction during plow operation is calculated as follows:

$$\begin{aligned} F &= (T_1+T_2)\cos\gamma + (N_1+N_2)\sin\gamma + \\ &+ \frac{1}{2}ks^2\sin\varepsilon\sin\gamma + \frac{ab\gamma}{g}v_e{}^2(1-\phi\cos\beta') + \\ &+ \frac{1}{\cos\beta - f\sin\beta}\left[(T_0+fI)e^{f\theta} + f\left(\frac{ab\gamma}{g}v_e{}^2\sin\varepsilon\sin\gamma + \frac{1}{2}ks^2\right)\right] \end{aligned} \tag{27}$$

From the above analysis, it can be seen that the resistance of the plough body working in the soil is mainly related to the angle ε, γ and β, and also related to the shape of the curved surface.

2.4 Determination of Structural Parameters of High-Speed Plow Body

As a traditional soil cultivation machine, the spar plow has a very important role in the development of Chinese agricultural machinery. Fig. 4 below shows the spar plow, which is connected to the tractor by its own suspension mechanism in the process of operation, relying on the tractor's power source to drive the spar plow to move in the soil in the process of operation, completing the periodic cutting and squeezing of the soil to turn over the soil.

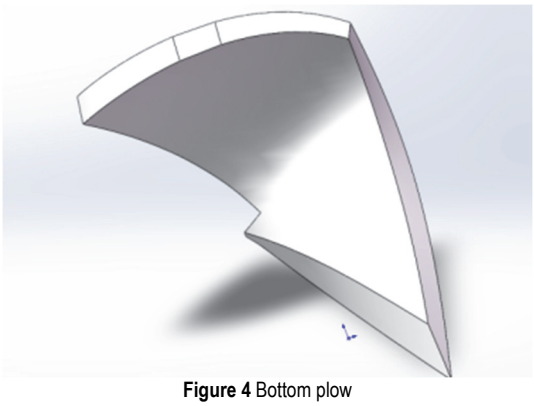

Figure 4 Bottom plow

The plow has a history of 2000 years in China. In the process of operation, the soil is turned over by cutting and squeezing the soil to achieve the turning of insect eggs and fertilizer on the surface to the lower layer of the soil, which can eliminate insect pests and weed cover and provide a good environment for the growth of crops while achieving soil loosening. The plow body is mainly composed of plowshare, plow wall, plow rest, plow column, plow side plate, etc. Each part plays its own role in the process of plow operation. When the plow body is plowing, the

plowshare cuts the soil and carries it up to the plow wall, which breaks the soil and turns it over.

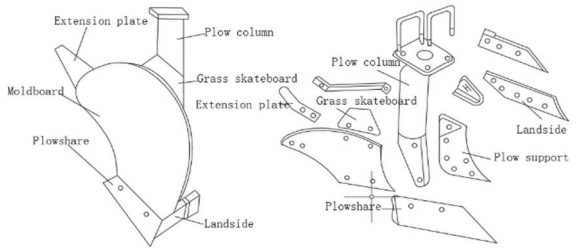

Figure 5 Schematic diagram of plow body structure

In the process of plow operation, the shape of the surface is determined by the guide curve. The parameters affecting the guide surface mainly include the opening and height h, as well as the angle ω formed by the tangent line of the starting and ending points of the plow share, and the angle ε formed by the starting straight section S and the X-axis of the pear share installation, as shown in Fig. 6. During the operation of the plow body, as different soil particles have different trajectories this also determines the working resistance of the plow body during operation. According to the relevant experience for the selection of parameters, the ratio of the height of the guide curve to the opening degree is about 1.7 ~ 1.8; the installation angle of the plowshare $\varepsilon = 20° \sim 30°$; the straight line of the lower part of the wire is taken as 6 cm; the larger the ω angle is in the process of guide curve operation, the greater the distortion of the plow body wings will be, the better the operation process for the turning performance of the soil fa, the more obvious the impact on the plowing resistance, in the process of design, take ω =105° ~ 109°. Take the plowing depth a = 250 mm, the plowing width b = 320 mm, the width-depth ratio $k = b/a$ = 1.28.

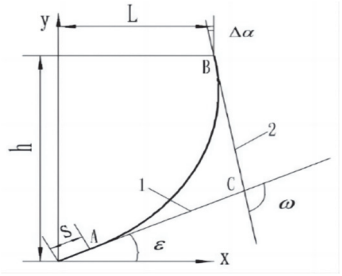

Figure 6 Guide curve

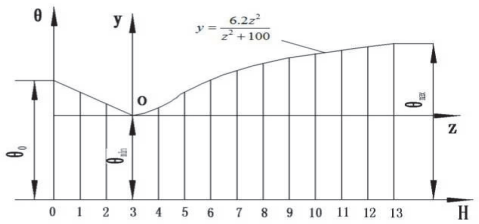

Figure 7 Rule of line element angle of broken soil plow surface

The pushing angle γ, also known as the metric line foot, is the angle between the plowshare edge line and the ditch wall, which is expressed in the form of a straight line that can be obtained by using a plane parallel to the ground against the intercepted horizontal straight metric line plow body surface, the straight line and the foot of the ditch wall as shown in Fig. 7.

It can be seen from Fig. 7 that θ_0 is the initial metaline angle, and its value range is 38° to 45°, in the process of ploughing operation, the cutting edge cuts out the soil at θ_0 angle, and under the action of continuous soil cutting extrusion, the element line angle is reduced to $\theta_{\min}$ during the rise of the soil map.

The second curve changes according to the law of the following Eq. (28), and the element line angle increases from $\theta_{\min}$ to $\theta_{\max}$, corresponding to the highest $H_{\max}$ of the plough body.

$$y = \frac{6.2z^2}{z^2 + 100} \tag{28}$$

The metric angle of each metric line can be obtained from Eq. (29):

$$\theta = \theta_{\min} + m\frac{6.2z^2}{z^2 + 100} \tag{29}$$

where m is the scale factor of each elementary line angle with respect to y. From Eq. (30), we have:

$$m = \frac{\theta_{\max} - \theta_{\min}}{y_n} = \frac{\Delta\theta}{y_n} \tag{30}$$

2.5 High-Speed Plow Body Mathematical Modeling

2.5.1 Mathematical Model of Guide Curves

Line 1 and line 2 in Fig. 1 to Fig. 6 can be obtained from the geometric relationship shown in Eq. (31) and Eq. (32):

$$1 : y = x \cdot \mathrm{tg}\varepsilon \tag{31}$$

$$2 : y = h + (l - x) \cdot \mathrm{tg}(90° - \Delta\alpha) \tag{32}$$

The coordinates of endpoints A and B obtained from the equations of lines 1 and 2 are respectively:

$$\begin{cases} x_A = S \cdot \cos\varepsilon \\ y_A = S \cdot \sin\varepsilon \end{cases} \tag{33}$$

$$\begin{cases} x_B = l \\ y_B = h \end{cases} \tag{34}$$

The coordinates of the intersection point C of straight line 1 and straight line 2 can be obtained by Eq. (32) and Eq. (33), which are found by calculating:

$$\begin{cases} x_C = \dfrac{h + l \cdot \mathrm{tg}(90° - \Delta\alpha)}{\mathrm{tg}\varepsilon + \mathrm{tg}(90° - \Delta\alpha)} \\ y_C = \mathrm{tg}\varepsilon \cdot \dfrac{h + l \cdot \mathrm{tg}(90° - \Delta\alpha)}{\mathrm{tg}\varepsilon + \mathrm{tg}(90° - \Delta\alpha)} \end{cases} \tag{35}$$

The line segments AC and BC are divided into the same n segments, then the coordinates of the mth point on the line segment AC are:

$$\begin{cases} px(m) = S\cdot\cos\varepsilon + \dfrac{m\cdot\left(h+l\cdot\mathrm{tg}\left(90^\circ-\Delta\alpha\right)\right)}{n\cdot\left(\mathrm{tg}\varepsilon+\mathrm{tg}\left(90^\circ-\Delta\alpha\right)\right)} - \dfrac{mS\cdot\cos\varepsilon}{n} \\ py(m) = S\cdot\sin\varepsilon + \dfrac{m\cdot\mathrm{tg}\varepsilon\left(h+l\cdot\mathrm{tg}\left(90^\circ-\Delta\alpha\right)\right)}{n\cdot\left(\mathrm{tg}\varepsilon+\mathrm{tg}\left(90^\circ-\Delta\alpha\right)\right)} - \dfrac{mS\cdot\sin\varepsilon}{n} \end{cases} \tag{36}$$

The coordinates of the mth point on the line segment BC are:

$$\begin{cases} Qx(m) = S\cdot\cos\varepsilon - \dfrac{m\cdot\left(h+l\cdot\mathrm{tg}\left(90^\circ-\Delta\alpha\right)\right)}{n\cdot\left(\mathrm{tg}\varepsilon+\mathrm{tg}\left(90^\circ-\Delta\alpha\right)\right)} + \dfrac{ml}{n} \\ Qy(m) = S\cdot\sin\varepsilon + \dfrac{mh}{n} - \dfrac{m\cdot\mathrm{tg}\varepsilon\left(h+l\cdot\mathrm{tg}\left(90^\circ-\Delta\alpha\right)\right)}{n\cdot\left(\mathrm{tg}\varepsilon+\mathrm{tg}\left(90^\circ-\Delta\alpha\right)\right)} \end{cases} \tag{37}$$

Making a horizontal line at height $z(j)$ intersecting with lines 1 and 2 above can be found by finding the horizontal coordinates of the intersection point as:

$$\begin{aligned} x(j,n) = {} & S\cdot\cos\varepsilon + \frac{m\cdot\left(h+l\cdot\mathrm{tg}(90^\circ-\Delta\alpha)\right)}{n\cdot\left(\mathrm{tg}\varepsilon+\mathrm{tg}(90^\circ-\Delta\alpha)\right)} - \frac{mS\cdot\cos\varepsilon}{n} + \\ & + \frac{\left[z(j)-Pz(m)\right]}{Sz(m)-Pz(m)}\cdot\left(\frac{ml+mS\cdot\cos\varepsilon}{n} - \frac{2m\cdot\left(h+l\cdot\mathrm{tg}(90^\circ-\Delta\alpha)\right)}{n\cdot\left(\mathrm{tg}\varepsilon+\mathrm{tg}(90^\circ-\Delta\alpha)\right)}\right) \end{aligned} \tag{38}$$

Connect each corresponding point on line 1 and line 2, respectively, and get the minimum value in this group, i.e., you can get the value of the opening of the derivative curve corresponding to the metric line j. The coordinates are:

$$\begin{cases} x(j) = x(j,n)_{\min} \\ z(j) = \Delta h\cdot j \end{cases} \tag{39}$$

2.5.2 Mathematical Model Expressions for High-Speed Plow Bodies

When the coordinates of the intersection of the jth straight element line and the guide curve are $xG(j)$ and $yG(j)$, the following geometric relationship can be obtained from the top view of the plough body (as shown in Fig. 8):

$$\begin{aligned} & \mathrm{Z} = \mathrm{Z}(j) \\ & xG(j) = OO'\cdot\cos\theta_0 + x(j)\cdot\sin\theta_0 \\ & yG(j) = OO'\cdot\sin\theta_0 - x(j)\cdot\cos\theta_0 \end{aligned} \tag{40}$$

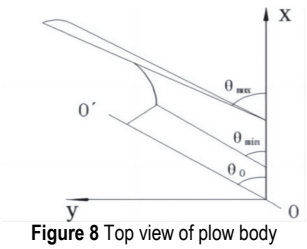

Figure 8 Top view of plow body

The figure shows that θ_0 is the initial metaline angle, and $\theta_{\min}$ and $\theta_{\max}$ are the minimum and maximum metaline angles, respectively.

After the processing of the expression, the surface metaline expression can be obtained as:

$$\begin{cases} \mathrm{Z} = \mathrm{Z}(j) \\ Y = Y(j) = yG(j) + \mathrm{tg}\theta(j)\cdot\left[X(j) - xG(j)\right] \\ X = X(j) = \left[y(j) - yD(j) + \mathrm{tg}\theta(j)\cdot xG(j)\right]/\mathrm{tg}\theta(j) \end{cases} \tag{41}$$

In this paper, the travel speed, plowshare installation angle, pushing angle and tangent angle of the two end points of the guide curve, which affects the resistance of the plowshare during operation, are optimized to suit the nature of the soil and the depth of tillage, so as to optimize the plowshare and reduce the tillage resistance of the plow body during operation.

2.5.3 High-Speed Plow Solid Model Creation and Output

The plow model is drawn using Solidworks and the design steps are shown below:

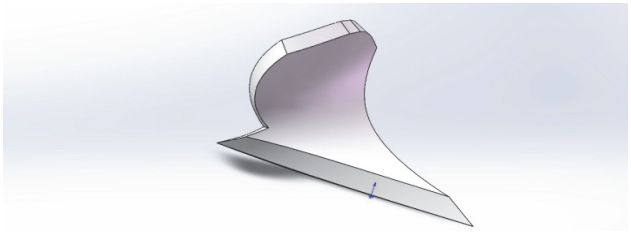

Figure 9 High-speed plow body model

In this paper, only the plowshare mounting angle of 25° is taken in the design process. The initial element line angle θ is 37°. The tangent angle edge of the two end points of the guide curve is 107° to establish the plow body model, and similar models are drawn in this way, and the plow body model is saved as the stp. format for export.

3 DISCRETE ELEMENT METHOD SIMULATION ANALYSIS OF HIGH-SPEED PLOW BODY STRUCTURE AND WORKING PARAMETERS ON TILLAGE RESISTANCE

3.1 Parameters Formulation

In this paper, we use EDEM software for simulation, and after the establishment of soil model as well as plow body model and the boundary model, we analyze the force situation under different pushing angles (37°, 39°, 41°) of plowshare installation angles (25°, 27°, 29°) and different angles of tangent lines (105°, 107°, 109°) of two end points of guide curve to determine the optimal design solution, and also according to the A comparative analysis was made based on different travel speeds and the force conditions under the action of different plowing depths (200 mm, 250 mm, 300 mm).

In recent years, the joint simulation based on MBD and DEM multi-body dynamics has become an important tool for studying agricultural machinery. This chapter analyzes the resistance during the motion of the high-speed plow based on the multi-topic dynamics recurdyn and the

discrete element modeling software EDEM, imposes the motion constraints of the high-speed plow in recurdyn, and also establishes the soil model in edem to study the high-speed plow. The influence of the parameters of the plow (mounting angle, pushing angle and angle of the tangent line at the two end points of different guide curves) on the resistance to motion is investigated, and based on the optimal parameters obtained, the resistance analysis under different conditions of speed and depth of entry is studied.

3.2 RD Model Building

3.2.1 Three-Dimensional Model Creation

This subsection focuses on using RD to constrain the motion of the high-speed plow as well as to apply motion functions, while using EDEM discrete element software to build the correct soil model.

In this paper, SW is used to build the 3D model of the high-speed plow and later change the different parameters, save STP or X_T to import into RD and determine the gravity direction as shown in Fig. 10 below:

Figure 10 Ploughshare mode

3.2.2 Motion Constraint Application

High-speed plough is mainly horizontal movement, using the Professional-Translate under the RD software, A moving vice was applied to the centroid of the high plough.

Figure 11 Speed applied

3.2.3 Imposition of the Motion Function

The software provides two methods of drive setting, which are standard drive method and user subroutine drive method. The standard drive method includes displacement (time) drive, velocity (time) drive and acceleration (time) drive.

In this paper, we choose the velocity (time) drive in the standard drive method, and the drive function is the 3rd polynomial approximation step function, which can better match the working process of high-speed plow acceleration motion and then uniform motion. The expression of the 3rd polynomial approximation step function is: STEP (x, x_0, h_0, X_8, h_1), and its meaning is:

When, $x \le x_0$,

$\mathrm{STEP} = h_0$;

When, $x_0 \le x \le x_1$

$$\mathrm{STEP}=h_0+(h_1-h_0)\left[(x-x_0)/(x_1-x_0)\right]^2\left\{3-2\left[(x-x_0)/(x_1-x_0)\right]\right\}$$

When, $x \ge x_1$

$\mathrm{STEP} = h_1$.

where x is the independent variable; x_0 is the starting value of the independent variable; X_8 is the ending value of the independent variable; h_0 is the starting value of the function; h_1 is the ending value of the function.

Meanwhile, the high-speed plow designed in this paper imposes the function STEP (Time, 0, 0, 1, 500), meaning that the model increases its speed to 0.5 m/s from 0 to 1 s, and then moves at a uniform speed.

3.3 EDEM Model Creation

Soil particle modeling in EDEM to build discrete element simulation models. Complex soil particle structure models can be built using 3D modeling software (e.g., solidworks, Pro/E, etc.) and imported into EDEM, while the particle module that comes with EDEM software can also generate simpler structure models directly by setting particle parameter sizes. According to the reference literature, the soil particles selected in this paper can be simplified to spheres for modeling, and their average diameter is 2.01 mm. The soil particles used in this paper are built by setting the particle size parameters in EDEM to model spherical particles with a diameter of 2.01 mm. The spherical particles are shown in Fig. 12.

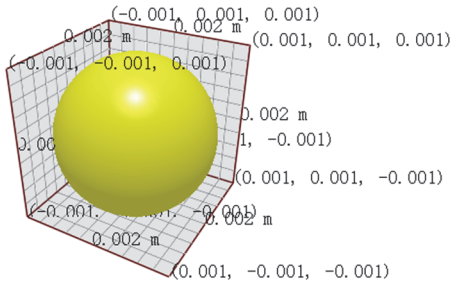

Figure 12 Soil particle mode

Table 2 Discrete element simulation parameter

Parameters	Cultivated soil
Radius of soil particles / mm	5
Poisson's ratio of soil	0.40
Soil shear modulus / Pa	1.00 × 106
Soil Density / kg/m³	1300
Recovery coefficient between soil particles	0.21
Static friction coefficient between soil particles	0.68
Coefficient of dynamic friction between soil particles	0.27
Recovery coefficient between soil and high-speed plow	0.39
Static friction coefficient between soil and high-speed plow	0.32
Coefficient of kinetic friction between soil and high-speed plow	0.08

The final establishment of the particle bed with length, width and height of 8 m, 0.4 m and 0.5 m is shown in Fig. 2 to Fig. 4 below.

3.4 Parametric Optimization

This subsection focuses on the relationship between the influence of high-speed plows on resistance at different installation angles, pushing angles and the angle of the tangent line between the two end points of the guide curve, and to obtain the optimal parameters, the joint defense model is shown in Fig. 13:

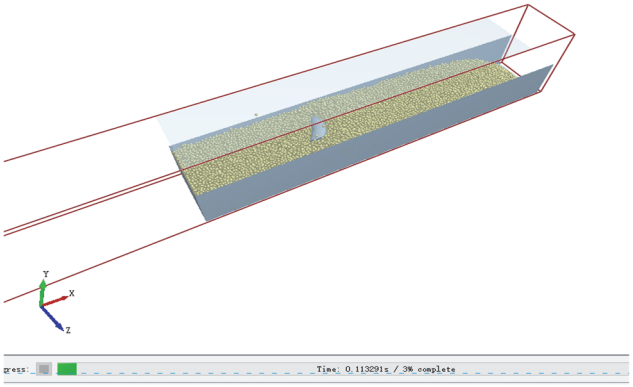

Figure 13 Joint simulation

According to the design of the high-speed plow and the actual working conditions, the speed and the depth of entry are 5 km/h and 300 mm. Based on the design principle, the values of the mounting angle, the pushing angle and the tangential angle of the two end points of the guide curve are taken as the direct horizontal resistance and the vertical resistance, which affects the operational performance of the high-speed plow. The angle of installation (25, 27, 29), the angle of pushing (37, 39, 41) and the angle of the tangent line between the two end points of the curve (105, 107, 109) is taken for analysis. The horizontal resistance and vertical resistance were taken as evaluation indexes, which were expressed as X_8, X_9, X_{10}, Y_3, Y_4, and three levels were selected for each factor, and a three-factor, three-level orthogonal combination test was designed, and the factor level table is shown in the following Tab. 3:

Table 3 Orthogonal combination table

Level	Factors		
	Mounting angle ε / °	Bulldozing angle γ /°	The angle between the tangents of the two endpoints of the guide curve ω / °
−1	25	37	105
0	27	39	107
1	29	41	109

3.5 Simulation Results Analysis

In the particle window bed, after setting the recurdyn and EDEM parameters, set the simulation time in recurdyn to (5) s and the step size to (0.01), start the simulation, and after the simulation is completed, in the recurdyn post-processing, read the horizontal resistance, vertical resistance, and the data are organized in the following Tab. 4.

Table 4 Simulation result

Plow Experiment Data No.	Test Serial No.	A	B	C	Test result		
		Ploughshare installation angle	Bulldozing angle	The angle between the tangents of the two endpoints of the curve			
		ε / °	γ / °	ω / °	Horizontal resistance / N	Vertical resistance / N	Buckling resistance / N
14	1	25	37	105	601.94	327.66	1223.15
15	2	25	37	107	660.92	349.85	1281.71
21	3	25	37	109	606.26	315.43	1310.41
6	4	25	39	105	580.54	385.93	1252.96
16	5	25	39	107	630.23	322.04	1321.77
10	6	25	39	109	595.47	287.30	1260.47
17	7	25	41	105	636.72	272.13	1308.83
5	8	25	41	107	576.66	312.43	1223.13
18	9	25	41	109	604.86	309.79	1237.19
7	10	27	37	105	582.78	313.14	1197.42
19	11	27	37	107	577.21	276.99	1257.38
8	12	27	37	109	614.64	291.71232	1268.96
20	13	27	39	105	642.99	284.26	1282.79
9	14	27	39	107	617.77	304.30	1266.67
22	15	27	39	109	624.96	258.98	1344.95
23	16	27	41	105	625.70	319.70	1314.39
24	17	27	41	107	633.10	335.67	1311.21
25	18	27	41	109	596.06	279.15	1217.79
26	19	29	37	105	589.77	270.80	1231.30
12	20	29	37	107	655.99	311.36	1260.91
27	21	29	37	109	601.64	301.48	1234.26
11	22	29	39	105	593.88	272.77	1254.63
28	23	29	39	107	608.43	301.94	1281.66
13	24	29	39	109	690.54	583.08	1280.59
15	25	29	41	105	617.79	290.90	1179.04
29	26	29	41	107	607.71	293.87	1242.87
30	27	29	41	109	624.11	295.94	1260.66
Plow Experiment Data No.	Test Serial No.	X_8	X_9	X_{10}	Y_3	Y_4	Y_5

A quadratic multiple regression was fitted to the data in the above table to obtain the quadratic multiple regression equation of the horizontal resistance to each independent variable as:

$$y_3 = 90643.452 - 2135.209x_8 + 1669.867x_9 - 1776.339x_{10} + 9.07x_8^2 - -18.83x_9^2 + 6.87x_{10}^2 + 1.106x_8x_9 + 15.155x_8x_{10} - 2.151x_9x_{10}$$

The quadratic multiple regression equation of vertical resistance on each independent variable was obtained as:

$$y_4 = -301109.799 + 3777.404x_8 - 1638.557x_9 + 5336.49x_{10} - -21.602x_8^2 + 28.1x_9^2 - 21.009x_{10}^2 + 0.046x_8x_9 - 24.8x_8x_{10} - 5.175x_9x_{10}$$

The quadratic multiple regression equation of the buckling resistance on each independent variable was obtained as:

$$y_5 = 28005.019 - 1368.829x_8 + 511.035x_9 - 363.384x_{10} + 6.624x_8^2 - -7.406x_9^2 + 0.601x_{10}^2 + 1.993x_8x_9 + 8.734x_8x_{10} + 0.107x_9x_{10}$$

3.6 Parametric Optimization

According to the above analysis, it is clear that the values of mounting angle ε, pushing angle γ and tangential angle ω at the two end points of the guide curve have taken directly horizontal resistance as well as vertical resistance, thus affecting the efficiency of the high -speed plow. During the numerical analysis, Y_3 and Y_4 are programmed in Matab to take $\omega \in [105, 109]$, $\varepsilon \in [25, 29]$ and $\gamma \in [37, 41]$ for the analysis.

The optimization analysis process is to find the combination with the minimum horizontal resistance/vertical resistance M within the variation of the installation angle ε, the pushing angle γ and the tangential angle ω at the two end points of the guide curve.

The following figure shows the horizontal resistance curve when ε is taken as 37, 39, 41. From the curve, it is clear that the horizontal resistance increases with the increase of the pushing angle, while the increasing trend of 39 - 41 is greater than the range of 37 - 41. The horizontal resistance of the height plow decreases first and then increases with the increase of the plowshare installation angle. When the plowshare installation angle ε is between 26 - 29, the horizontal resistance decreases slowly and then increases again, which has less influence on the horizontal resistance, while ω is more stable at 107 - 109.

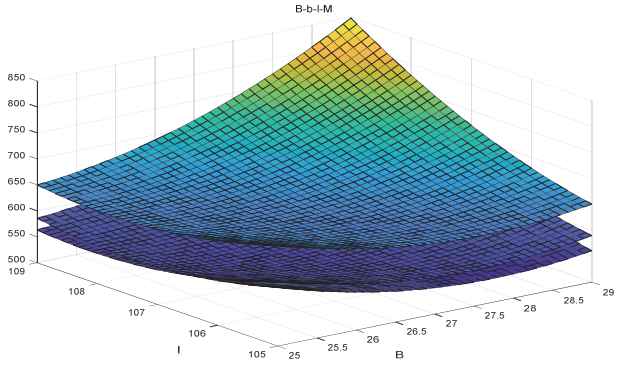

Figure 14 Simulation results

The following figure shows the vertical resistance curve when γ takes 37°, 39° and 41°. From the curve, it can be seen that the vertical resistance increases slowly with the increase of pushing angle, while the rising trend of 39° - 41° is less than the range of 37 - 49. The vertical resistance of height plow decreases with the increase of plowshare mounting angle. When the plowshare installation angle is between 26° - 29°, the vertical resistance decreases slowly and then flattens out, while at a higher level of installation angle, the effect on vertical resistance is less, while the ω is more stable at 107° - 109°. When the ω is at a high level, the vertical resistance is smaller.

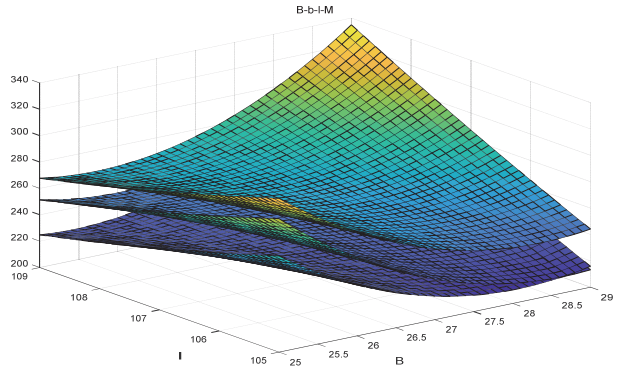

Figure 15 Simulation result

To summarize the analysis shown above, the installation angle ε the pushing angle γ and the tangent angle ω at the two end points of the guide curve are optimized by taking the interval values according to the simulation results, while the horizontal resistance as well as the vertical resistance is used as evaluation indicators, and the traversal solution idea is applied to find the optimal parameters of the high-speed plow:

Min $[y_3(\varepsilon, \gamma, \omega), y_4(\varepsilon, \gamma, \omega)]$, $\varepsilon \in [105, 109]$, $\gamma \in [25, 29]$, $\omega \in [37, 41]$

The optimal combination is solved for (27, 39, 108), while the horizontal resistance is 627.88 N, the vertical resistance is 333.72 N, and the buckling resistance is 1195.11 N.

3.7 Study of Different Simulation Conditions for High-Speed Plows

In the previous section, the installation angle ε the pushing angle γ and the tangential angle ω at the two end points of the guide curve are optimized mainly by using the horizontal resistance as well as resistance of the vertical as evaluation indicators to determine the best design parameters. In this subsection, the simulation analysis of the high-speed plow was carried out mainly based on the best parameters obtained by optimization, under different working conditions with speeds of (8, 9, 10) km/h and plowing depths of (20, 25, 30) cm, to study the effect of resistance on the high-speed plow under different settings.

Simulation results are as follows.

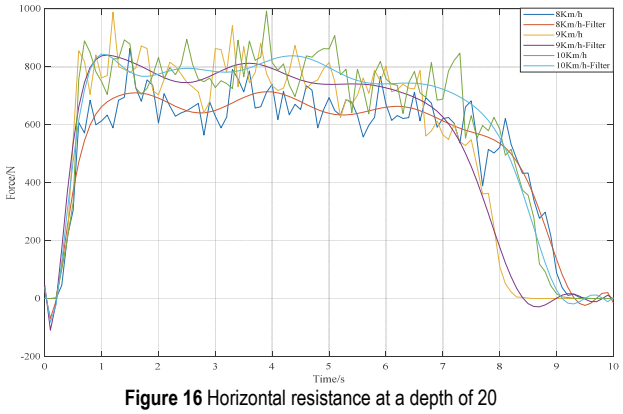

Figure 16 Horizontal resistance at a depth of 20

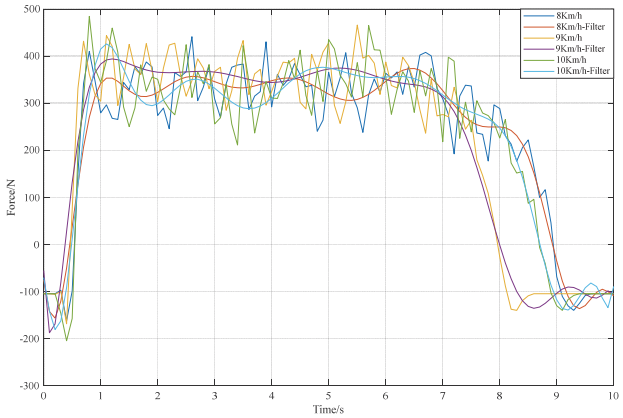

Figure 17 Vertical resistance at a depth of 20

The above two graphs show horizontal resistance and vertical resistance at a plowing depth of 20 cm and speeds of 8 km/h, 9 km/h and 10 km/h. For data visibility, the data was filtered and the graphs show that the horizontal resistance and vertical resistance increase with speed, while the increase in vertical resistance from 8 km/h to 9 km/h is less than that from 9 km/h to 10 km/h.

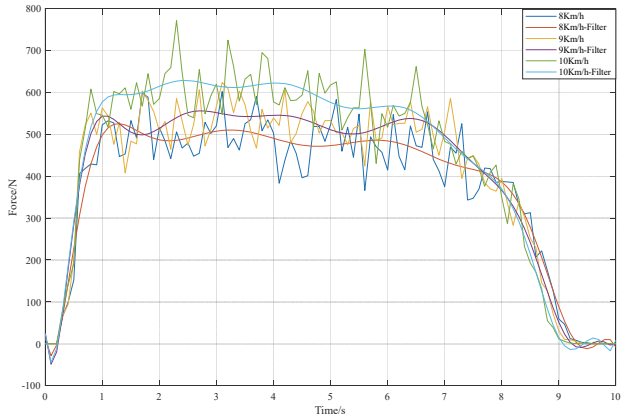

Figure 18 Horizontal resistance at a tilage depth of 25

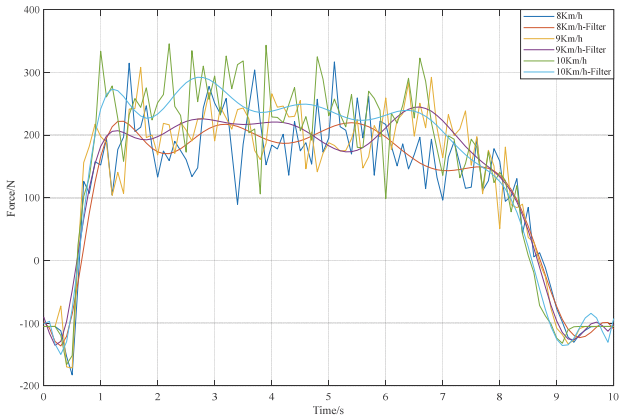

Figure 19 Vertical resistance at a plowing depth of 25 cm

Under the working condition of plowing depth of 25 cm, it is known from the horizontal resistance and vertical resistance curve: with the increase of speed, the horizontal resistance increases in turn, meanwhile, the vertical resistance decreases first and then increases, and at 9 km/h, the vertical resistance is the smallest, which is 300 N.

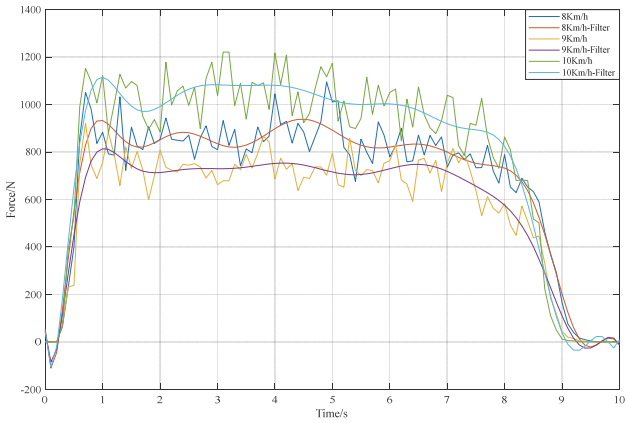

Figure 20 Horizontal resistance with a tillage depth of 30 cm

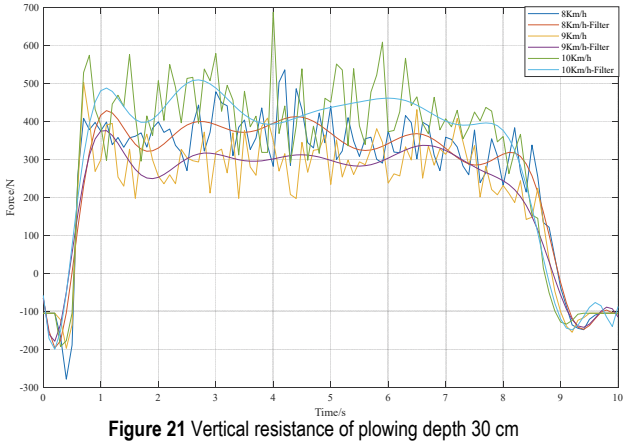

Figure 21 Vertical resistance of plowing depth 30 cm

In the plowing depth of 30 cm working conditions, by the horizontal resistance, vertical resistance curve can be seen: with the increase of speed, the horizontal resistance first decreases and then increases, at the same time, the vertical resistance first decreases and then increases, at 9 km/h, the horizontal resistance and vertical resistance are the smallest, respectively, 700 N, 300 N

In summary: when the operating depth is 30, the speed is 9 km/h, the vertical resistance is the smallest, where the speed is 9 km/h, plowing depth of 25 and 30, the vertical resistance is basically the same and the smallest, the value is 300 N, in the plowing depth of 20, the horizontal resistance is the smallest, and the horizontal resistance is greater than the vertical resistance. In the process of field test comparison, using the optimized plowshare, the tractive force is reduced by 10.62% at the speed of 9 km/h compared to plowshare before optimization.

3.8 EDEM Post-Processing Analysis

The following figure shows the velocity cloud of soil particles at different moments of the high-speed plow in the EDEM post-processing. The color range of the soil particles from white to green to red indicates the sequential increase of the disturbed soil velocity, taking a certain working condition as an example, and intercepting the soil particles with time.

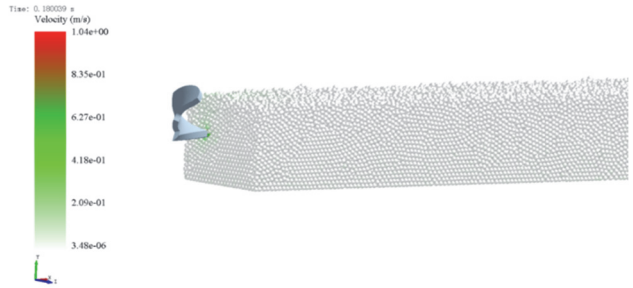

Figure 22 Contact phase force

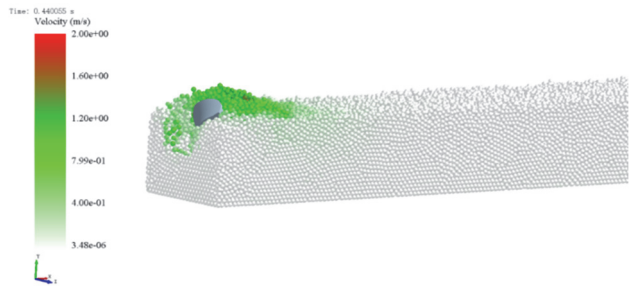

Figure 23 Force during the soil stage

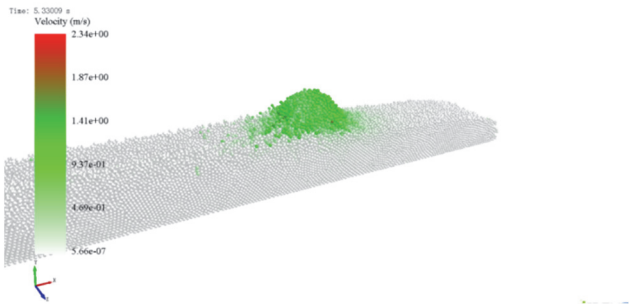

Figure 24 The state of motion is stressed

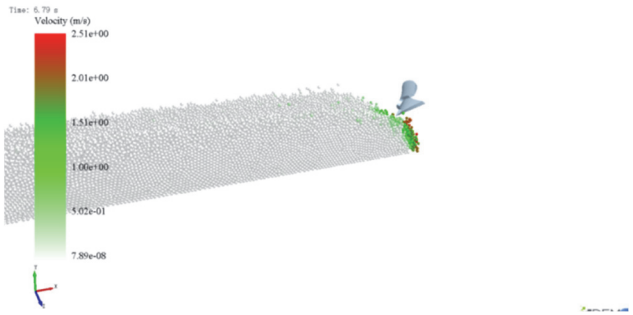

Figure 25 The departure stage is stressed

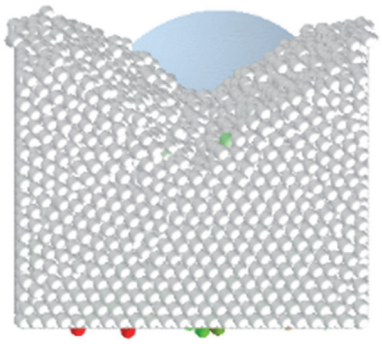

Figure 26 The departure stage is stressed

The above Fig. 22 to Fig. 26 show that: the high-speed plow just touches the soil in 0.18 s, the soil receives extrusion, so the local color turns from white to green, when it moves to 0.44 s, the high-speed plow has basically all entered the soil, the soil particles around the plow body become green, indicating that the soil is sheared by the plow body, while the horizontal resistance of the plow body as well as the vertical resistance increases continuously. In 0.44 s - 6.79 s, the plow body moves in the soil while disturbing and turning the soil and opening the furrow, which plays a good effect of turning the soil, while the soil is all submerged in the plow body, the horizontal resistance and vertical resistance is the largest, at the end of 6.79 s, the plow body all leaves the soil, the speed of the soil gradually decreases, while the soil particles in the graph show red, indicating that due to inertia, the higher speed of the soil with the plow body height movement is taken out, which is in line with the actual movement effect.

4 FIELD TRIALS

4.1 Field Trial Programs

With tillage speed (8 km/h, 9 km/h, 10 km/h), tillage depth (200 mm, 250 mm, 300 mm) as the test factors and tillage resistance as the test index, a single-factor test method was used to study the effect of each factor on the tillage resistance of the high-speed plow and whether each performance index met the requirements. The test factor level was 3. The field test of the high -speed plow is shown in Fig. 27, and the data are collected and collated by telemetry to obtain the tillage resistance of the high-speed plow during operation.

Figure 27 Force analysis

4.2 Field Performance Trials

The test program can be obtained according to the division of tillage depth and tillage speed level, as shown in Tab. 5. The tillage resistance data are noted after each group of tests to be measured after its operating quality, soil breaking rate and vegetation cover meet the relevant requirements is accurate, and the test methods for these performance indicators are shown below, with reference to GB/T14225-2008 "Spar Plow".

Table 5 Test plan table

Test No.	Plowing depth/ mm	Plowing speed/ km/h
1	200	8
2	200	9
3	200	10
4	250	8
5	250	9
6	250	10
7	300	8
8	300	9
9	300	10

Table 6 Field test data of high-speed plough

Plowing depth / mm	Plowing speed / km/h	Results of field trials					
		Coefficient of variation of tillage depth stability / %	Coefficient of variation of tillage width stability / %	Vegetation and stubble coverage below 8 cm / %	Soil breakage rate / %	Simulation of traction resistance / N	Actual traction resistance / N
200	8	3.0	4.2	84.2	81.7	1332.72	1456
200	9	3.3	7.4	84.4	85.4	1438.69	1502.31
200	10	4.1	4.5	84.3	80.0	1559.36	1623.5
250	8	4.2	4.6	87.3	86.9	1963.38	2012.3
250	9	3.5	3.2	87.6	87.2	1925.02	1950.23
250	10	3.1	5.2	87.3	85.5	2263.25	2421.02
300	8	4.4	3.8	85.9	85.7	2626.15	2800.12
300	9	4.9	4.4	86.3	84.8	2741.2	2903.12
300	10	5.3	4.0	84.2	83.2	3040.72	3102.35

4.3 Experimental Results and Analysis

The data of each test result measured in the field test operation of the high-speed plow according to the test program are shown in Tab. 6.

According to the following test results and analysis, after each group of tests, the performance indexes of the plow meet the relevant requirements. In order to more clearly reflect the changes in the operating indexes of the high-speed plow by plowing depth and operating speed, the following line graph is made.

When the plowing depth is 200 mm, the coefficient of variation of plowing depth stability and the coefficient of variation of plowing width stability of the high-speed plow at different operating speeds were plotted as line graphs, as shown in Fig. 28.

As can be seen from Fig. 28, when the plowing depth is 200 mm and 300 mm, the coefficient of variation of plowing stability of the plow body increases with the increase of speed, and the plowing depth is not stable enough, with a linear relationship; when the plowing depth is 250 mm, the coefficient of variation of plowing stability decreases in speed, which means that under a certain plowing depth, the faster the speed the better the plowing stability. The stability of plowing width under different speed and plowing depth is different, when the plowing depth is small, the coefficient of variation of plowing width stability first becomes larger and then decreases, with the increase of plowing depth, the coefficient of variation of plowing width stability increases slightly, and the operating speed is 9 km/h under the condition that the plowing depth is 250 m more stable.

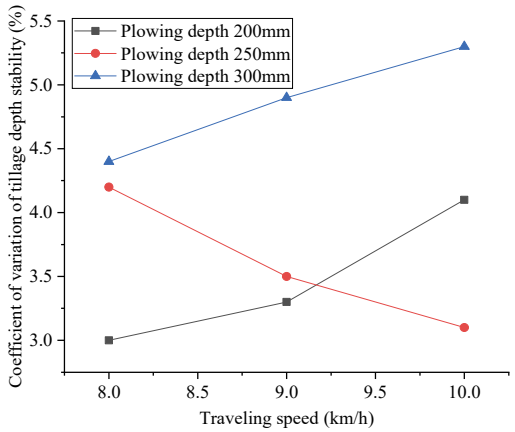

a) Coefficient of variation of tillage depth stability at different tillage depths and travel speeds

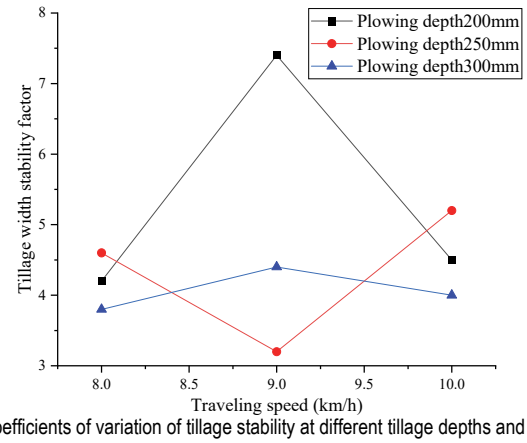

b) Coefficients of variation of tillage stability at different tillage depths and travel speeds

Figure 28 Stability coefficient of variation of tillage depth and tillage width under different tillage depth and tillage speed

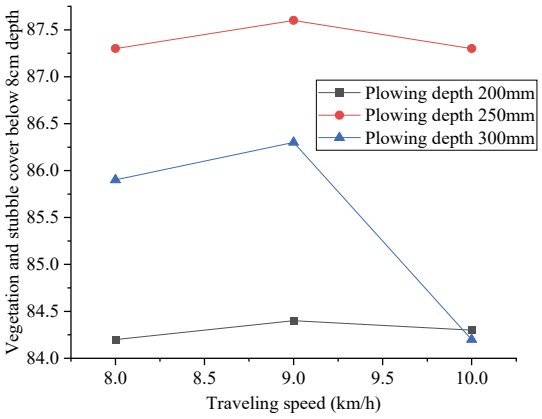

a) Vegetation and stubble coverage below 8 cm depth at different cultivation depths and travel speeds

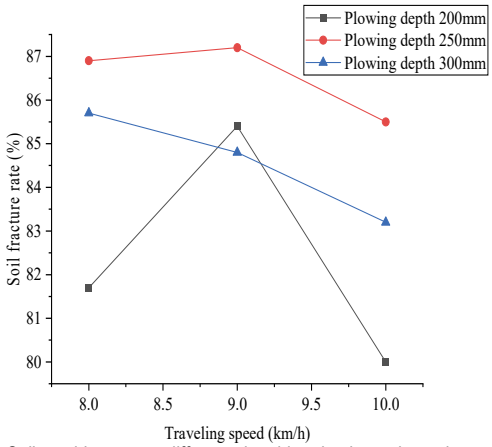

b) Soil crushing rate at different ploughing depths and travel speeds

Figure 29 Vegetation and stubble coverage rate below 8cm at different depth and speed

From Fig. 29, it can be seen that the vegetation and stubble cover below 8 cm depth increases and then decreases with the increase of speed, and the cover is worse in the case of larger speed, and the cover also increases and then decreases slightly with the increase of plowing depth as a whole, and the vegetation and stubble cover below 8 cm depth is generally higher in the state of plowing depth 250 mm, and the best result is achieved under the condition of operating conditions speed of 9 km/h. The best results were achieved at an operating speed of 9 km/h.

When the plowing depth was 200 mm and 250 mm, the rate of soil fragmentation increased and then decreased with the increase of speed, and the best result was achieved at the plowing depth of 250 mm and the operation speed of 9 km/h. However, under the condition of 300 mm, the rate of soil fragmentation kept decreasing with the increase of speed.

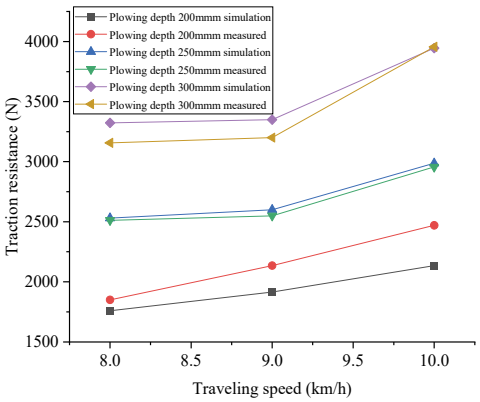

Figure 30 Traction drag at different tillage depths at different speeds

As can be seen from Fig. 30, under the influence of different operating speeds, the traction resistance shows an increasing state. However, at 9 km/h, the traction resistance shows a slight decrease, reducing the resistance and improving the production efficiency.

5 CONCLUSION

Based on recurdyn + EDEM simulation, the following results are obtained:

1. The horizontal resistance and vertical resistance under different working conditions of high speed plough, and optimize the interval value based on the installation angle, push le and both ends of the guide curve to obtain the optimal parameters (27, 39, 108), the horizontal resistance is 627.876 N, vertical resistance is 306.11 N and the buckle resistance is 1195.11 N.
2. Based on the optimal parameters of the resistance analysis at different tillage depths and speeds, it can be obtained: the horizontal resistance increases successively with the speed of 20 cm, but under the tillage depth of 25 cm, the horizontal resistance decreases first and then increases with the speed. Under the condition of 20 cm, the compression resistance of the soil increases with the increase of velocity. In depth of a high level, the vertical resistance decreases and then increases as the speed increases, and the horizontal resistance is always greater than the vertical resistance.
3. The maximum error between the theoretical traction value and the measured traction value is 9.3%, and the simulation shows the force situation of the actual operation. With the simulated tillage depth of 20 cm, 25 cm and 30 cm respectively, and the tillage speed of 8, 9 and 10 km/h, the minimum horizontal and vertical resistance at the tillage rate of 9 km/h is obtained.
4. After analyzing the coefficient of variation of tillage width stability, coefficient of tillage depth stability, vegetation and stubble coverage rate below 8 cm depth and crushing rate, it is high when the tillage speed of 25 cm is 9 km/h. At this time, compared with the traditional share plough at the depth of 25 cm, the traction resistance is reduced by 10.86% at the speed of 9 km/h.

6 REFERENCES

[1] Lixin, Z. (2011). *Study on the influence of plough structure and working parameters on tillage resistance of rheotropic soil*. Nanjing Agricultural University,

[2] Kushwaha R. (1990). A non-linear 3-D finite element analysis of soil failure with tillage tools. *Journal of Terramechanics*, *27*(4), 341-966. https://doi.org/10.1016/0022-4898(90)90033-I

[3] Fielke, J. M. (1999). Finite Element Modelling of the Interaction of the Cutting Edge of Tillage Implements with Soil. *Journal of Agriculture Engineering Researeh*, *74*, 91-10. https://doi.org/10.1006/jaer.1999.0440

[4] Gao, Q., Pitt, R. E., & Ruina, A. A. (1986). A model to predict soil forces on the plough mouldboard. *Journal of Agricultural Engineering Research*, *35*, 141-155. https://doi.org/10.1016/S0021-8634(86)80053-1

[5] Araya, K., Kodho, M., Zhao, D., Liu, F., & Jia, H. (1995). Improvement of Planosol Solum: Part 2, Optimization of Design of Roll-In Ploughs in Soil Bin Experiments. *Journal of Agricultural Engineering Research*, *63*, 261-268. https://doi.org/10.1006/jaer.1996.0028

[6] Baker, B. (2009). Deep-sea monsters. *The engineer*, *294*(772), 21-22.

[7] Harrison, H. P. (1982). Soil Reactions from Laboratory Studies with an Inclined Blade. *Transactions of the ASAE*, *25*(1), 7-12. https://doi.org/10.13031/2013.33466

[8] Shen, X. & Wang, P. (1996). Analysis of the force and its application. *Xinjiang Agricultural Science and Technology*, *2*, 46-51.

[9] Feng, X. (2004). *Intelligent CAD system and CAE study of plough frame*. Jilin University

[10] Liao, L., Yang, J., & Meng, S. (2011). Simulation analysis of operation process of crushed plough surface-Based on ANSYS/S-DYNA. *Agricultural mechanization research*, *33*(4), 9-12.

[11] Gee-Cough, D., Wang, J., Kanok-Nukucha, W. (1994). Deformation and Failure in Wet Clay Soil: Part 3, Finite Element Analysis of Cutting of Wet Clay by Tines. *Journa of Terramechanics*, *58*, 121-131. https://doi.org/10.1006/jaer.1994.1042

[12] Ma, T. & Lu, X. (1993). The force spiral action point on the plough surface is determined by analysis. *Journal of Beijing Agricultural Engineering University*, *13*(04), 47-53.

[13] Wang, X. & Xue, H. (1998). Analysis of plough force and calculation and correction of force. *Journal of Heilongjiang Bayi Agricultural Reclamation University*, *1998*(03), 29-32.

[14] Ying, Y., Zhao, Y., & Zhang, Q. (1994). Question and computer-aided analysis of the traditional force analysis method of hanging plough. *Journal of Agricultural Machinery*, *1994*(03), 61-65.

[15] Zhao, R. & Wang, B. (1992). Calculation method for force analysis of hanging plough. *Journal of Beijing Agricultural Engineering University*, *12*(02), 15-23.

[16] Zhang, J., Wang, W., Ni, M., et al. (2014). Static stress analysis of plough surface based on six split force test. *Xinjiang agricultural mechanization*, *164*(02), 15-18.
[17] Coyne, J. C. & Lewis, G. W. (1999). Analysis of plowing forces for a finite-width blade in dense, ocean bottom sand. *Oceans Conference Record (IEEE)*, 1-10.
[18] Dong, X., Ma, R., & Wang, I. (2023). Design of the experimental teaching platform for the working mechanism of intelligent agricultural equipment based on open-source hardware. *Experimental technology and management*, 1-8.
[19] Sun, Y. (2022). Design of conveying fan. *Agricultural machinery use and maintenance*, *2022*(12), 17-19.
[20] Liu, M., Hu, C., & Xie, B. (2022). Optimization analysis and test of split-share plough simulation based on discrete element method. *Zhejiang Journal of Agriculture*, 3*4*(11), 2542-2552.
[21] Xiao, J., Yang, X., Xia, G., Li, W., & Hou, Q. (2021). Study on the wear resistance of laser cladding Fe-Mo coating. *Special Steel Technology*, *27*(04), 13-17+12.
[22] Li, Q., Zheng, X., Meng, X., Liu, J., Zhang, L., & Liang, Y. (2021). Application status and improvement suggestion of share share plough in northern Xinjiang. *China Agricultural Machinery Chemistry Journal*, *42*(07), 202-208.
[23] Hongbo, J. (2021). Analysis of common problems in the share plough test. *Jiangsu Agricultural Mechanization*, *2021*(01), 26-28.
[24] You, A., Zhou, T., Mo, Y., Wu, Z., Hu, L., & Chen, Y. (2020). Improvement of rear rear plpost. *Hubei Agricultural Mechanization*, *2020*(18), 125-126.
[25] Liu, F., Sun, Y., Gao, Y., Dou, J., Hou, Z., Wan, C., Liu, H., Wang, L. (2019). Spatial distribution characteristics of straw in share plough and hydraulic amplitude regulation. *Hubei Agricultural Science*, *58*(23), 57-60.
[26] Song, F., Liu, Y., Bing, K., Zhang, S., & Qiao, X. (2019). In situ overturned plough design based on TRIZ theory. *China Agricultural Machinery Chemical News*, *40*(04), 13-18.
[27] Yi. F., Shi, J. D., Yang, G., & Ma, Y. (2019). Research and application of the share plough. *China Agricultural Machinery and Chemical News*, *40*(03), 231-236.
[28] Deng, T., Chang, Y., Zhao, Y., Chen, C., An, C., Zheng, X. (2018). Optimization study on biomimetic improvement of the share plough surface. *Journal of Jilin Agricultural Science and Technology University*, *27*(01), 116-117.

Contact information:

Xin ZHENG
(Corresponding author)
College of Engineering, Heilongjiang Bayi Agricultural University,
Daqing Heilongjiang, 163319, China
E-mail: zhengxin_hbau@163.com

Wenbao XU
College of Engineering, Heilongjiang Bayi Agricultural University,
Daqing Heilongjiang, 163319, China

Hengyan XIE
College of Engineering, Heilongjiang Bayi Agricultural University,
Daqing Heilongjiang, 163319, China